ORIGIN OF TWO DISTINCT POPULATIONS IN DWARF SPHEROIDAL GALAXIES

Daisuke Kawata[1,2], Nobuo Arimoto[3], Renyue Cen[4], and Brad K. Gibson[2,5]
Submitted to ApJ

ABSTRACT

We study the chemical and kinematic properties of the first galaxies that formed at high redshift, using high resolution cosmological numerical simulations, and compare them with the recent observational results for the Sculptor dwarf spheroidal galaxy of Tolstoy et al., who found two distinct stellar populations: the lower metallicity stars are more spatially extended and possess a higher velocity dispersion than the higher metallicity stars. Our calculations reproduce these observations as the result of a steep metallicity gradient within a single population, induced by dissipative collapse of the gas component. We also predict strong [N/O] enhancements in the lowest metallicity stars in dwarf spheroidals, due to the preferential retention of ejected gas from intermediate-mass stars, compared to Type II supernovae.

Subject headings: galaxies: abundances — galaxies: kinematics and dynamics —galaxies: formation —galaxies: stellar content — galaxies: individual (Sculptor)

1. INTRODUCTION

Dwarf galaxies in the Local Group are one of the prime observational targets for galactic astronomy because their relatively short distances enable us to observe the properties of individual stars, which provide many details of their formation history (Baade 1944). Dwarf Spheroidals (dSphs) are one of the most populous dwarf galaxy types seen in the Local Group and are defined as galaxies with $M_B > -14$ mag, low surface brightness ($\mu_V > 22$ mag arcsec^{-2}), no well-defined nucleus (although in some dSphs, such as Fornax and Sagittarius, a globular cluster seems to correspond to a nucleus), and very little gas (Gallagher & Wyse 1994; Grebel 1997; Mateo 1998). They do not have any ongoing star formation. Some of them do not have any intermediate-age stars at all. On the other hand, our current favorite Λ-dominated cold dark matter (ΛCDM) cosmology suggests that small objects form first, and larger systems are built up by the assembly of smaller systems (e.g., White & Rees 1978). Therefore, it is considered that dSphs might be the first generation of galaxies and survived cannibalization by larger systems. Hence, dSphs might contain a record of the epoch of the end of the dark age. Recently, using a cosmological numerical simulation, Ricotti & Gnedin (2005) demonstrated that the small galaxies formed at high redshifts can explain the global properties, such as the luminosity, velocity dispersion, and iron abundance, of the dwarf galaxies observed in the Local Group. Their study encourages us to undertake further investigation of the connection between the first galaxies and the dSphs.

With the wide-field multi-object spectrograph FLAMES on the Very Large Telescope, Tolstoy et al. (2004, hereafter T04) have measured the metallicity and line-of-sight velocity for 300 member stars, distributed over a large radial range (~ 20 times its core radius), in the Sculptor (Scl) dSph galaxy. They found that the stars in the Scl dSph show two distinct populations. One of them is more metal rich ([Fe/H]~ -1.4) with a centrally concentrated distribution. The other one is metal-poor ([Fe/H]~ -2) and more spatially extended. In addition, the higher metallicity stars show lower velocity dispersion than the lower metallicity stars. This is unprecedented information for unveiling the formation history of the Scl dSph.

To disentangle the formation process of the dSph from such observational data, we construct a theoretical model that can be compared with the observations. The aim of this paper is to show our first attempt to make a self-consistent numerical simulation model that can be compared with the observational data of the Scl dSph directly and quantitatively. We pay particular attention to the radial trend of iron abundance and velocity dispersion, which are not discussed in Ricotti & Gnedin (2005), for comparison with the unprecedentedly detailed observation presented in T04. The next section describes our numerical method. Section 3 presents our simulation results and comparison with the observational data in T04. Our discussion and conclusions are given in Section 4.

2. NUMERICAL METHODS

In this study we focus on the properties of a dwarf galaxy that formed at a high redshift in our high-resolution cosmological simulation. The simulation was carried out using the galactic chemodynamics code `GCD+` (Kawata & Gibson 2003a). `GCD+` is a three-dimensional tree N-body/smoothed particle hydrodynamics (SPH) code that incorporates self-gravity, hydrodynamics, radiative cooling, star formation, supernova (SN) feedback, and metal enrichment. `GCD+` takes account of chemical enrichment by both Type II (SNe II) and Type Ia (SNe Ia) SNe and mass loss from intermediate-mass stars, and follows the chemical enrichment history of both the stellar and gas components of the system. To study the

[1] The Observatories of the Carnegie Institution of Washington, 813 Santa Barbara Street, Pasadena, CA 91101
[2] Swinburne University of Technology, Hawthorn VIC 3122, Australia
[3] National Astronomical Observatory, 2-21-1 Osawa, Mitaka, Tokyo 181-8588
[4] Department of Astrophysical Sciences, Princeton University, Peyton Hall, Ivy Lane, Princeton, NJ 08544
[5] Centre for Astrophysics, University of Central Lancashire, Preston, Pr1 2HE, United Kingdom

formation process of small systems, we update the code to implement non-equilibrium chemical reactions of hydrogen and helium species (H, H^+, He, He^+, He^{++}, H_2, H_2^+, H^-) and their cooling processes. The details of the updated code are described in the Appendix A.

We adopt a ΛCDM cosmology of $\Omega_0 h^2 = 0.135$, $\Lambda_0 = 1 - \Omega_0$, $\Omega_b h^2 = 0.0224$, and $h = 0.71$ (Spergel et al. 2003), and use a multi-resolution technique (Kawata & Gibson 2003b) to achieve high-resolution in the regions of interest, while outer regions exerting the tidal forces are handled with lower resolution. The initial conditions for the simulations are constructed using the public software GRAFIC2 (Bertschinger 2001). Gas dynamics and star formation are included only within the relevant high-resolution region (~ 80 kpc in comoving scale); the surrounding low-resolution region (~ 530 kpc diameter sphere) contributes to the high-resolution region only through gravity. Consequently, the initial condition consists of a total of 287,491 dark matter particles and 233,280 gas particles. The mass and softening length of individual gas and dark matter particles in the high-resolution region are 129 650 $M_\odot$ and 30 and 51 pc, respectively.

To reduce the computational cost, we applied a significantly small simulation volume. Hence, our simulation misses the density perturbation induced by larger scale modes. Figure 1 demonstrates that the mass variance $\sigma(M)$ becomes slightly smaller at the mass scale in which we are interested ($\sim 10^8 M_\odot$) if the power spectrum for wavelengths longer than our simulation volume are ignored. In addition, the first galaxies are expected to form at high-density peaks, i.e. biased regions (Mo & White 1996). Therefore, we adopt a higher value of $\sigma_8 = 1.8$, instead of the value suggested by recent observations ($\sigma_8 = 0.9$). Figure 1 also shows the mass variance for the applied power spectrum. The adopted high σ_8-value enables us to form a relevant dSph-like small galaxy in the particular realization with the relatively small simulation volume, in addition to partly compensating for the missing waves larger than our simulation box.

In the high-resolution region, we find a small stellar system at $z = 5.9$ (Figure 2). The virial radius and mass of this system are respectively 1.9 kpc and $5.1 \times 10^7 M_\odot$ at $z = 5.9$. Here, we follow the fitting formula in the Appendix of Kitayama & Suto (1996) to define the virial mass and radius, taking into account the cosmology and redshift. We assume that at this redshift, star formation in this system has been quenched by mechanisms, such as re-ionization (e.g., Efstathiou 1992; Chiba & Nath 1994; Thoul & Weinberg 1996; Bullock et al. 2000; Benson et al. 2002; Susa & Umemura 2004b) and/or galactic wind (e.g., Dekel & Silk 1986; Arimoto & Yoshii 1987), and that the system evolves passively afterwards. Thus, we assume that the chemical and kinematic properties at $z = 5.9$ would not change until $z = 0$, and we analyze the properties expected at $z = 0$ from the output of the simulation at $z = 5.9$. This is, of course, consistent with our assumption that the observed dSph is a galaxy that formed early and retained its own identity until z=0. We check this *Ansatz* by examining its detailed properties.

The middle panel of Figure 2 shows the rest-frame V-band luminosity distribution of this galaxy at $z = 5.9$.

The luminosity distribution is calculated by our population synthesis code, taking account of the metallicity and age of the star particles at $z = 5.9$. We use the single stellar population spectrum data in Kodama & Arimoto (1997). The data do not include any emission lines. For simplicity, we do not take into account any absorption by the inter-stellar (ISM) and inter-galactic medium (IGM). To make sure that the system is dynamically stable and that the distribution of stellar population and kinematics does not change dramatically until $z = 0$, we run a pure N-body simulation using the particles within a radius of ~ 1.7 times the virial radius at $z = 5.9$, as an initial condition. We run this N-body simulation (relaxing run) for about 5 Gyr (corresponding to the time from $z = 5.9$ to $z = 1$). The right panel of Figure 2 shows the rest-frame V-band luminosity distribution analyzed from the final output of this relaxing run extrapolated at $z = 0$, based on the stellar age at $z = 0$. Figure 3 shows the V-band surface brightness profiles for the system before (*open circles*) and after (*filled circles*) the relaxing run. The profile after the relaxing run is similar to the profile before. We also confirm that all the properties presented in this paper are not changed after the relaxing run. Therefore, the properties at $z = 5.9$ are expected to be unchanged till $z = 0$. We present only the results from the data after the relaxing run in the next section.

The above relaxing run does not explicitly include the effects of two-body relaxation, because the system's stellar density is so low that its effects are not dominant. We have derived the total number of stars within the virial radius, N_s, the velocity dispersion, σ_0, and the number density of stars, $n_{s,0}$, taking into account the initial mass function (IMF) and the remnant stars, in the central region, and obtained $N_s \sim 6.5 \times 10^5$, $\sigma_0 \sim 10$ km s^{-1} and $n_{s,0} \sim 0.005$ pc^{-3} with a mean stellar mass of about $m_* = 0.3$ $M_\odot$. The two-body relaxation time can then be estimated as (e.g., Ogorodnikov 1965)

$$t_r = \sigma_0^3/(4\pi G^2 m_*^2 n_{s,0} ln N_s). \tag{1}$$

This leads to $t_r = 7.0 \times 10^{14}$ yr, suggesting that two-body relaxation is not important for this system.

The solid line in Figure 3 represents a King profile with the same core radius r_c and tidal radius r_t as observed in the Scl dSph, i.e. $r_c = 0.12$ kpc and $r_t = 1.6$ kpc. We assume that the distance of the Scl dSph is 72 kpc (Kunkel & Demers 1977, T04). The central surface brightness is normalized to roughly match the simulated surface brightness profile. In the inner region, the simulated system has a profile similar to the observed profile of the Scl dSph, which means that the simulated galaxy has a similar core radius. In the outer region, the simulated galaxy has a higher surface brightness compared to the King profile. Therefore, the tidal radius of the simulated galaxy is inconsistent with the observed one. However, our simulated galaxy is an isolated system, while the Scl dSph is a satellite galaxy of the Milky Way. We expect that if the simulated galaxy falls into a bigger host galaxy, the stars in the outer region are tidally stripped, and thus that the tidal radius would depend on their environment, which could make the tidal radius of the simulated galaxy smaller and similar to the observed one. Here, we assume that such stripping does not change the properties of the inner region, and compare the properties of this isolated system with those of
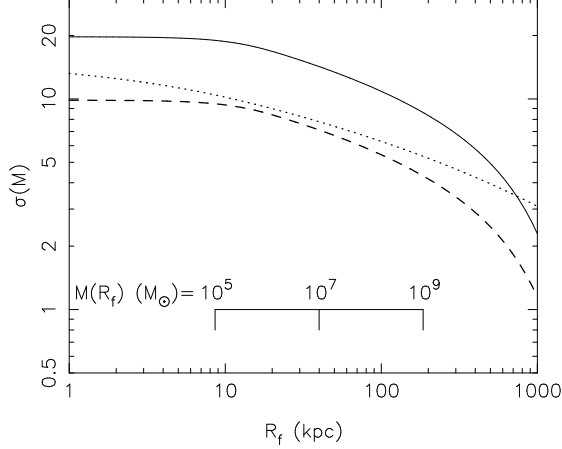
Fig. 1.— The mass variance for the CDM power spectrum as a function of filter radius, R_f. The mass corresponding to the filter radius, $M(R_f)$, is also shown in the panel The dotted line shows the mass variance with $\sigma_8 = 0.9$. The dashed line indicates the same as dotted line, but the power spectrum for the wave-length longer than our simulation volume (~ 530 kpc) and shorter than Nyquist wave-length (~ 22 kpc) are ignored. The solid line demonstrates the same as the dashed line, but with $\sigma_8 = 1.8$, i.e. our applied power spectrum.

the Scl dSph.

The basic properties of the simulated galaxy are summarized in Table 1. In the next section, we compare our model results with the observational data of the Scl dSph in T04.

3. RESULTS

Figure 4 shows the formation history of this galaxy. Although some minor mergers are involved, the system forms through smooth accretion. The lower panel of Figure 5 shows the virial mass evolution of the galaxy and building blocks that merge into the galaxy. The panel demonstrates that the main system experiences only two minor mergers (mass ratio smaller than 0.4). The top panel of Figure 5 shows the history of the star formation rate (SFR). In this galaxy, star formation starts at $z = 25.5$ and the SFR has a peak around $z = 15$. The $z = 17.8$ panel in Figure 4 shows that the gas is blown out and the heavy elements are distributed to the IGM. Table 2 presents the heavy-element mass budget for the stars that are within the virial radius at $z = 5.9$. The total ejected mass $M_{Z,\mathrm{ej}}$ means the mass of each heavy element ejected from stars within r_{vir} until that redshift. The mass in the stellar component, $M_{Z,\mathrm{s}}$, is defined as the mass of each heavy element still within the stellar component within the virial radius. We define the escape fraction as $f_{\mathrm{esc}} = 1.0 - M_{Z,\mathrm{s}}/M_{Z,\mathrm{ej}}$. Here we assume that the heavy elements in the gas component are also blown out after some mechanism stops star formation at $z = 5.9$. Table 2 indicates that more than 96% of the heavy elements produced in stars have escaped from the system until $z = 5.9$. Our assumed SNe feedback (7.5×10^{50} erg per supernova, which is chosen to reproduce the low metallicity of the Scl dSph) has a strong effect on the gas dynamics and continuously blows out the gas from the system. However, the continuous gas accretion leads to further star formation, albeit at a somewhat lower rate. Figure 5 shows that star formation continuously occurs

even around this blow-out phase. Nevertheless, the star formation of this small system is strongly suppressed by SNe feedback, which helps to keep the stellar metallicity low, as seen in the age-metallicity relation shown in the right panel of Figure 6.

As described in Section 1, T04 found that the stars in the inner region have higher metallicity than those in the outer region. They split the two regions at a radius of about 0.25 kpc and demonstrated that the metallicity distribution function (MDF) of stars in the inner (outer) region has a peak around [Fe/H]$= -1.4$ (-2.0). To compare with their result, Figure 7 shows the MDF for stars in the inner ($R < 0.25$ kpc[6]) and outer (R>0.25 kpc) regions for our simulated galaxy. The MDF for the inner (outer) region of the simulated galaxy has a peak at [Fe/H]~ -1.4 ([Fe/H]~ -1.9), which is in good agreement with the observed MDFs in T04. Therefore, the simulated galaxy also show two distinct stellar populations.

We found that this is simply due to the metallicity gradient in the system. Figure 6 shows that the peak of the metallicity distribution at different radii gradually decreases as the radius increases, i.e., that there is a metallicity gradient in the simulated system. Since the metallicity gradient is steep enough in the system, the MDF for the inner region moves toward higher [Fe/H], compared to the MDF for the outer region. This demonstrates that the steep metallicity gradient can cause two different chemical properties in the inner and outer regions.

Next, we analyze the kinematic properties. Figure 8 presents the velocity dispersion at different radii for the low-metallicity ([Fe/H]< -1.7) and high-metallicity ([Fe/H]> -1.7) stars. This velocity dispersion is obtained by taking the line-of-sight velocity dispersion of stars within annuli at different radii. To improve the statistics, we analyzed the line-of-sight profiles at 36 different projections, and obtained the mean values and dispersions, which are represented as error-bars in the figure. Figure 8 also shows the observed velocity dispersion of the low-metallicity ([Fe/H]< -1.7) and high-metallicity ([Fe/H]> -1.7) stars in T04. Within a radius of about 0.6 kpc, the observational data show that the velocity dispersion of the high-metallicity stars is lower than that of the low-metallicity stars.[7] In other words, the two different metallicity components also have distinctive dynamical properties. Our simulation results also show the same trend. Although the difference is small, the difference is significant and more than twice that of the dispersions shown as the error bars in the inner region.

Our simulation demonstrates that a system formed at a high redshift can reproduce the two stellar populations whose chemical and dynamical properties are distinctive. However, the simulated galaxy shows some inconsistent results with the observed properties of the Scl dSph. First, compared with Figure 3 of T04, the MDFs for both inner and outer regions of the simulated galaxy have too long a tail at lower [Fe/H]. In the observational data,

[6] Throughout this paper, R represents radius at an arbitrary projection, and we ignore the stars $R > 2.5$ kpc.
[7] Note that T04 mentioned that in the region outside of the radius of 0.6 kpc, the number of the high metallicity stars are too small.
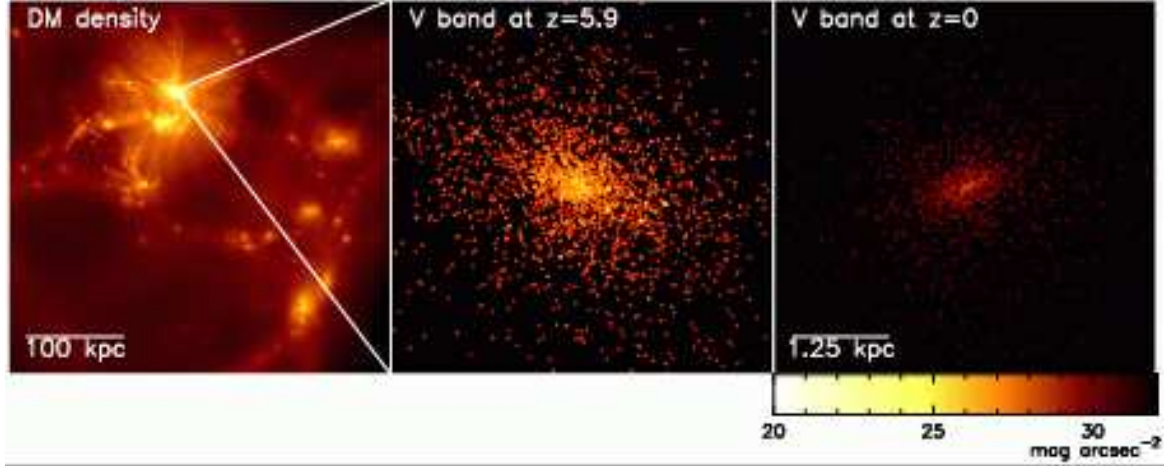
Fig. 2.— Dark matter density distribution at $z = 5.9$ (left), V-band (rest-frame) luminosity distribution at $z = 5.9$, and expected V-band luminosity distribution at $z = 0$ after the passive evolution.

TABLE 1
Basic Model Results

M_{vir} $(M_\odot)$	r_{vir} (kpc)	$M_{gas}(< r_{vir})$ $(M_\odot)$	$M_{DM}(< r_{vir})$ $(M_\odot)$	$M_{star}(< r_{vir})$ $(M_\odot)$	M_V (mag)	T_{vir}[a] (K)
5.1×10^7	1.9	3.5×10^5	5.0×10^7	1.9×10^5	-7.23	2.8×10^3

[a]Virial temperature calculated by $GM_{vir}\mu m_p/3k_B r_{vir}$ (Kitayama & Suto 1996).
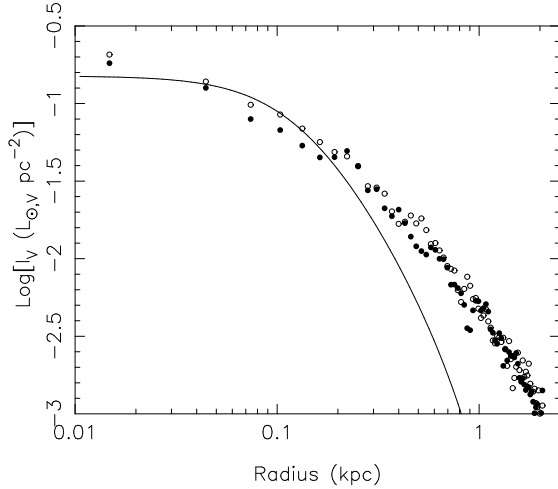
Fig. 3.— The V-band surface brightness profile from the simulation data before (open circles) and after (solid circles) the relaxing run (see text for details). The solid line presents a King profile with the core radius, $r_c = 0.12$ kpc, and tidal radius, $r_t = 1.6$ kpc.

TABLE 2
Heavy element mass budget for the system within R_{vir}.

	$z = 12.1$				$z = 5.9$		
	$M_{Z,ej}$[a] $(M_\odot)$	$M_{Z,g}$[b] $(M_\odot)$	$M_{Z,s}$[c] $(M_\odot)$	f_{esc}[d]	$M_{Z,ej}$ $(M_\odot)$	$M_{Z,s}$ $(M_\odot)$	f_{esc}[e]
N	17.0	7.6	0.26	0.55	160.0	7.2	0.96
O	170.0	57.0	1.3	0.66	1900.0	74.0	0.96
Fe	17.0	2.3	0.066	0.86	150.0	3.0	0.98

[a]Total ejected mass.
[b]Mass in gas component.
[c]Mass in stellar component.
[d]Escape fraction, $1 - (M_{Z,g} + M_{Z,s})/M_{Z,ej}$.
[e]Escape fraction, $1 - M_{Z,s}/M_{Z,ej}$.

there are no stars at [Fe/H]< -2.8, although T04 selected their samples from the limited region of the color-magnitude diagram, which might tend to exclude stars of too low and too high metallicity. On the other hand, the simulated galaxy has a significant fraction of stars with such low metallicity. Next, Figure 8 also shows that the velocity dispersion of our simulated galaxy is too small compared with the observed values. In addition, Table 1 shows that the V-band magnitude of the simulated galaxy ($M_V = -7.23$) is also small, compared with the

luminosity of the Scl dSph ($M_V = -10.7$). These are problems of our current model that need to be solved in a future study, and we discuss possible solutions in the next section.

Finally, we have also analyzed abundance ratios. Tolstoy (2005) shows that stars in the Scl dSph show different distributions in the [α/Fe] versus [Fe/H] plane, compared with the stars in the solar neighborhood (see also Shetrone et al. 2003; Geisler et al. 2005). In the Scl dSph, the [α/Fe] values of member stars with [Fe/H]< -2 are higher than solar abundance ratios, and [α/Fe] values approach the solar value as [Fe/H] increases at [Fe/H]> -2. On the other hand, in the solar neighborhood [α/Fe] values are constantly higher than the solar value for stars with [Fe/H]< -1 and starts decreasing at [Fe/H]$= -1$. This difference can be explained by the contribution from
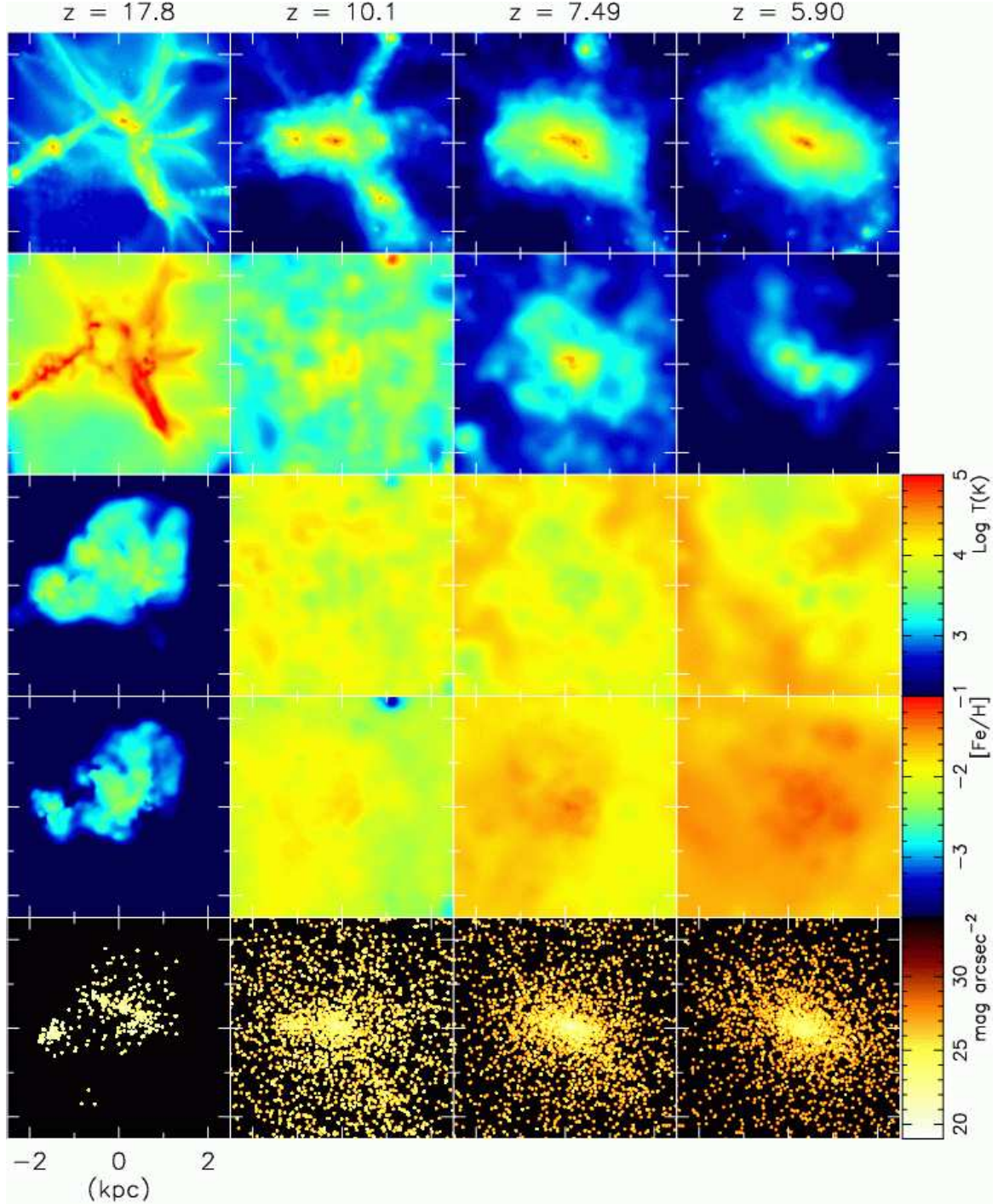
FIG. 4.— Evolution of the distributions of dark matter density (top), the gas density (2nd), the gas temperature (3rd), the iron abundance of gas (4th), and K-band (observed-frame) luminosity (bottom).

SNe Ia, which decreases $[\alpha/\mathrm{Fe}]$, and a lower star formation rate in the dSph, which keeps $[\mathrm{Fe/H}]$ low until the chemical enrichment by SNe Ia becomes important (e.g., Ikuta & Arimoto 2002; Lanfranchi & Matteucci 2003, 2004; Lanfranchi et al. 2005). However, Figure 9 demonstrates that in the simulated galaxy, the mean $[\mathrm{O/Fe}]$ is almost constant (oxygen is one of the typical α-elements). One reason why there is no enrichment from SNe Ia is because we implemented an SNe Ia model proposed by Kobayashi et al. (2000), who suggested that SNe Ia are

inhibited in stars with $[\mathrm{Fe/H}]< -1$. Even if we relax their $[\mathrm{Fe/H}]$ limit for SNe Ia, it is difficult to explain the observational trend. Kobayashi et al. (2000) consider that the mass ranges of companion stars for the SNe Ia progenitor binaries are restricted to between 0.9 and 1.5 $\mathrm{M_\odot}$ (they call this the RS+WD system) and to between 1.8 and 2.6 $\mathrm{M_\odot}$ (the MS+WD system). The expected lifetime of 2.6 $\mathrm{M_\odot}$ stars with $\mathrm{Log}(Z/Z_\odot)= -2.3$ are about 0.5 Gyr, according to the lifetime used in Kodama & Arimoto (1997). On the other hand, Figures 5 and 6 indicate
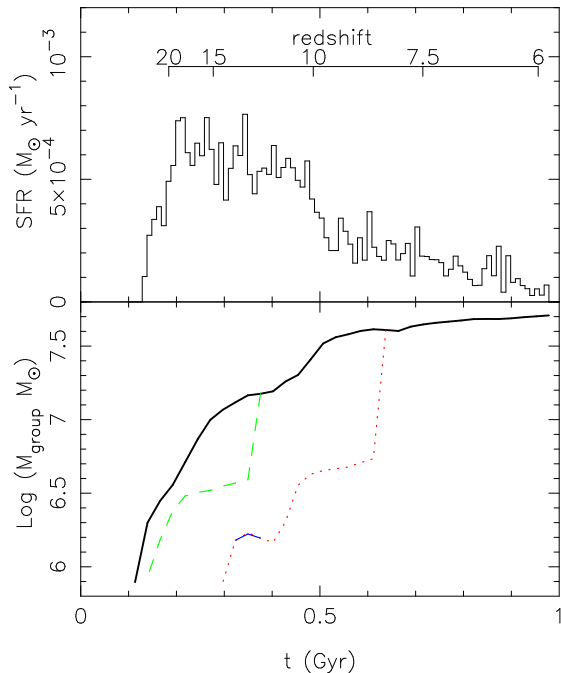
FIG. 5.— Time variation of the star-formation rate and the evolution of the virial mass of the progenitor halos. In the bottom panel, different styles of the lines (black thick-solid, red dotted, green dashed and blue thin-solid) indicate different halos. The connection between lines displays that two halos merge together. For example, the halo shown by red dotted line merges into the large halo described by black thick-solid line at $t \sim 0.64$ Gyr.

that stars with [Fe/H]> -2 start forming even 0.1 Gyr after the first star formation. However, the progenitors of SNe Ia are still unknown. For example, another SNe Ia progenitor model suggested by Greggio & Renzini (1983) suggests that the mass range of binaries is between 8 and 3 M$_\odot$. Since the lifetime of such stars is 0.03-0.3 Gyr, if we applied their model, the observational trend of [O/Fe] and [Fe/H] could be explained. Another solution to explain the decrease in [α/Fe] is increasing the contribution of SNe II from stars with masses between 10 and 15 M$_\odot$ whose yields provide [α/Fe]< 0 (e.g., Woosley & Weaver 1995; Gibson 1997). However, the observed trend of the decreasing [α/Fe] requires a fine-tuned variation of the shape of the IMF, depending on metallicity, which seems unlikely.

Figure 9 also shows that the simulated [O/Fe] has too large a scatter, compared with the observational data. The particles with a low [Fe/H] are likely enriched only a few times, and then their abundance pattern reflects that of the yields from the stars within a small mass range. As a result, the scatter of [α/Fe] for the star particles becomes as large as the [α/Fe] variation of the yields of SNe II progenitors with different masses (Woosley & Weaver 1995). This indicates a serious problem of the current chemical evolution model in particle-based numerical simulations. The problem is also known in explaining the small dispersion of [α/Fe] for metal-poor halo stars ([Fe/H]$= -3$ to -2) in the Milky Way, which provides a strong constraint to the chemical evolution history of the Galaxy (e.g., Arnone et al. 2005). So far, numerical simulations of disk galaxy formation show clearly larger scatter than what is observed (see also

Raiteri et al. 1996). This suggests that we have to consider some metal-mixing model between particles. Nevertheless, the mean values of metallicity from the current simulation models may be relatively robust.

We also analyzed the abundance ratio of [N/O] against [O/H] and found an interesting feature. Figure 10 demonstrates that there is a visible trend that [N/O] decreases from [N/O]$= 2$ to ~ 0 as [O/H] increases from [O/H]$= -4$ to -1.5. The middle panel of the figure also shows that high [N/O] are seen in the stars formed around $t = 0.3$ Gyr and that stars born at later epochs have lower [N/O] values. This high [N/O] comes from stars with masses between 4 and 8 M$_\odot$ whose lifetime is around 0.1 Gyr (Fig. 10, *right*). To make the contribution from such intermediate-mass stars important, we are required to suppress the contribution from higher mass stars whose [N/O] values are lower and whose lifetimes are shorter. As seen in Figure 4, the enriched gas is blown out at a high redshift around $z = 18$, due to the strong feedback by SNe II and the relatively shallow potential of the system at such a high redshift. As a result, chemical enrichment by massive stars, i.e. SNe II, becomes less important and enrichment from intermediate-mass stars becomes relatively more important. As the system becomes larger and the gravitational potential binds the gas enriched by SNe II, [N/O] starts decreasing. This is also demonstrated in Table 2, which shows the metal budget at $z = 12.1$ and $z = 5.9$. Note that since star formation is still in progress, the escape fraction at $z = 12.1$ is defined as $f_{esc} = 1.0 - (M_{Z,g} + M_{Z,s})/M_{Z,ej}$. Here, $M_{Z,g}$ is the mass of each heavy element still within the gas component within the virial radius. At $z = 12.1$, the escape fraction of oxygen is significantly higher than that of nitrogen, and the values become closer at $z = 5.9$. Oxygen is mainly produced in SNe II, although it is still created in the intermediate-mass stars (van den Hoek & Groenewegen 1997). On the other hand, nitrogen mainly comes from the intermediate-mass stars. Thus, Table 2 indicates that the gas enriched by SNe II is preferentially blown out at high redshift. Therefore, testing this trend of [N/O] in dSphs would be interesting. To our knowledge, the nitrogen abundance has not been observed in dSphs. On the other hand, the intermediate-mass stars are also expected to be progenitors of s-process elements. Recent observational studies (e.g., Smecker-Hane & McWilliam 2002; Tolstoy et al. 2003; Sadakane et al. 2004; McWilliam & Smecker-Hane 2005b,a) suggest that the s-process elements are enhanced in the dSphs. This might be explained by a process in dSph in which the SNe II-enriched gas is preferentially blown out of the system and the enrichment by intermediate-mass stars is more important. Interestingly, Smecker-Hane & McWilliam (2002); McWilliam & Smecker-Hane (2005a) have shown that the s-process elements are more enhanced in higher metallicity stars in the Sagittarius dSph. In addition, Sadakane et al. (2004) found a very metal-poor star ([Fe/H]$= -2.7$) that has an anomalously low abundance of s-process elements in the Ursa Minor dSph. This may indicate a delay of s-process element enrichment, because s-process elements come from relatively low-mass (1.5-3 M$_\odot$), i.e. long-lifetime, stars (see also Lanfranchi et al. 2005).
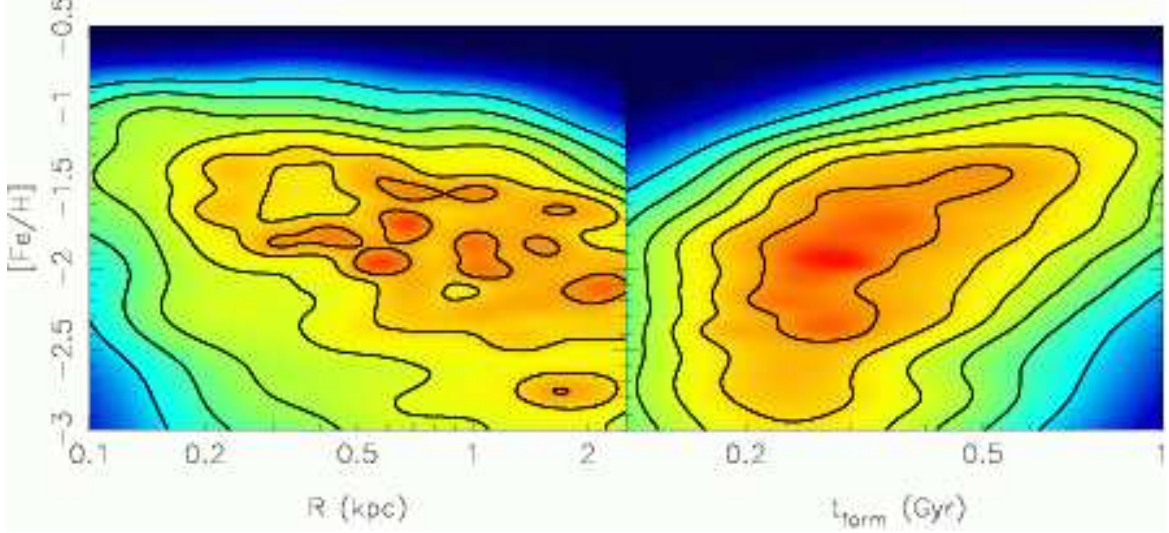
Fig. 6.— Smoothed stellar mass distribution in the [Fe/H] vs. radius plane (left) and in the [Fe/H] vs. formation time, t_{form}, plane, i.e. the age-metallicity relation (right).

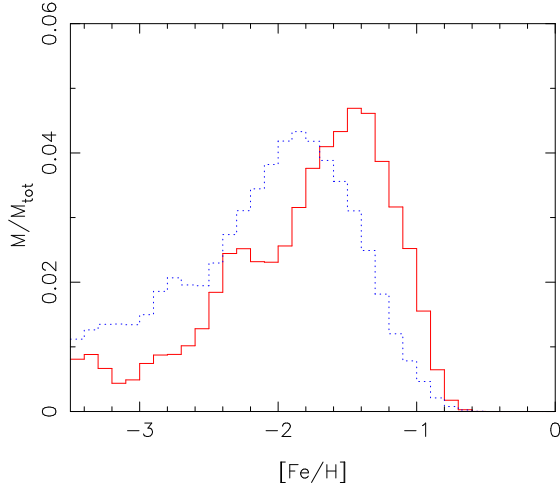Fig. 7.— Metallicity distribution function of stars in the inner ($R < 0.25$ kpc: red solid histogram) and outer ($R > 0.25$ kpc: blue dotted histogram) region.

Fig. 8.— Velocity dispersion profile of high ([Fe/H]> -1.7: red circles connected with solid line) and low ([Fe/H]< -1.7: blue triangles connected with dotted line) metallicity stars. The error-bars represent the dispersions from the measurements at the different projections. The observational data in T04 are also shown as the red solid (for [Fe/H]> -1.7) and blue dotted (for [Fe/H]< -1.7) crosses, where the horizontal-bar corresponds to the radial range, and the vertical-bar corresponds to their dispersion. The vertical-bars are plotted with an offset, for clarity.

4. DISCUSSION AND CONCLUSIONS

We have analyzed chemical and kinematic properties of a small system that formed at high redshift in a ΛCDM cosmological simulation. Our simulated galaxy shows that higher metallicity ([Fe/H]> -1.7) stars have a more centrally concentrated distribution and lower velocity dispersion, compared with the lower metallicity stars ([Fe/H]< -1.7). This trend is consistent with the observed trend in the Scl dSph reported in T04. Thus, we conclude that a survivor of a small system that formed at high redshift can explain the observed stellar chemical and kinematic properties.

T04 claim that this observed trend indicates that there are two distinct populations in the Scl dSph. They propose three possible mechanisms to explain the two populations. (1) Two episodes of star formation. Subsequent SNe feedback from the initial star formation blows out the gas and stops star formation temporally. After SNe
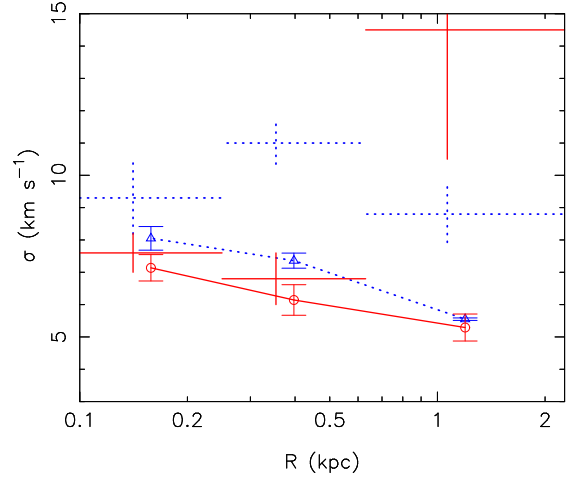
feedback becomes weaker, more metal-rich gas comes back and forms a new generation of stars (Carraro et al. 2001; Mori et al. 2002). (2) External influences, such as minor mergers or accretion of additional gas at a later epoch. (3) Selected heating by UV background radiation. The radiation evaporates the outer layers of the gas preferentially, and star formation lasts longer in the inner region (Susa & Umemura 2004a). Figure 5 shows that our simulated galaxy does not have two episodes of star formation. In this study, we assume that there is no later minor merger or gas accretion after star formation is stopped at high redshift, and star formation is abruptly terminated without any time delay depending on the radius. Thus, the formation history of our sim-
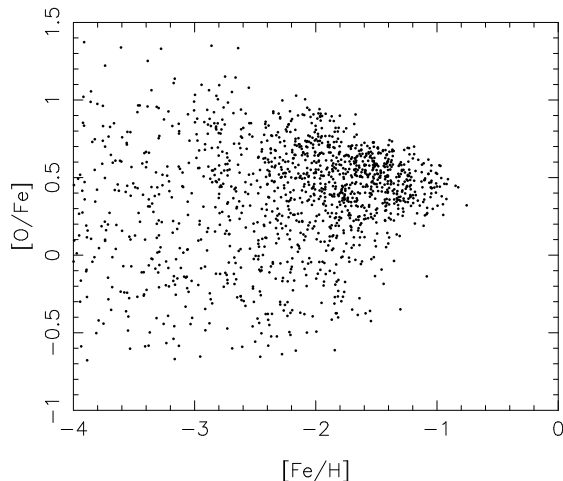
FIG. 9.— [O/Fe] as a function of [Fe/H] for star particles within $R = 2.5$ kpc.

ulated galaxy does not correspond to any of the above scenarios.

Figures 4 and 5 show that the simulated galaxy forms through smooth accretion rather than major mergers. It is known that such smooth accretion of the dissipative gas component leads to the higher metallicity for the gas in the inner region, because gas that dissipatively accretes into the inner region is enriched by stars in the outer region, as well as by stars in the inner region, where the stellar density is higher. As Figure 5 shows, the substantial duration of the starburst at $z = 13 \sim 20$ allows for significant self-enrichment in the inner region of the galaxy, resulting in a higher metallicity stellar population there. The outer regions are progressively less vigorous in star formation activities due to the supernova explosion feedback effect, which significantly reduces the gas content of the galaxy, as well as subsequent merger subunits. The latter point is clearly visible in Figure 5; for example, the merger event at $z \sim 8$ is not associated with any increased star formation activity, indicating a lack of gas. This mechanism makes the mean metallicity of the stars in the inner region higher. This is the same mechanism that is suggested to explain the metallicity gradient for larger spheroidals, i.e. normal elliptical galaxies (Larson 1974; Carlberg 1984; Kawata & Gibson 2003a; Kobayashi 2004). In fact, Figure 6 shows a metallicity gradient in the simulated system. Hence, our simulation demonstrates that for a small system that stopped forming stars at a high redshift, it is possible to have a metallicity gradient, which can explain the *apparent* two distinct populations observed in the dSph Scl stars. Note that the metallicity gradient has to be steep, to make such a difference in the inner and outer regions. Thus, if the steepness of the metallicity gradient is responsible for the apparent two populations in the dSph and metallicity gradients are different between dSphs, as seen between elliptical galaxies (e.g., Kobayashi & Arimoto 1999), there may be dSphs that do not show two such populations, due to a less steep metallicity gradient. Thus, it would be important to obtain more samples of both simulated and observed dSphs. However, here we also note that our simulation result does not rule out alternative scenarios

to explain the observed two populations, such as those discussed in T04.

Unfortunately, some properties of our simulated galaxy are inconsistent with those observed in the Scl dSph. Figure 7 shows that in both the inner and outer regions there are significant amounts of stars that have extremely low metallicity. This is the same problem as the so-called G dwarf problem, known from the difficulty for a simple chemical evolution model to explain the MDF of the G dwarfs in the solar neighborhood (e.g., van den Bergh 1962; Tinsley 1975) and to reproduce the spectrum features in the central region of bright elliptical galaxies (e.g., Arimoto & Yoshii 1987; Bressan et al. 1994; Greggio 1997). The solutions suggested for the solar neighborhood G dwarf problem include (1) gas infall, (2) prompt initial enrichment (PIE), and (3) metal-enhanced star formation (MESF). The infall model has so far been very successful in solving the local G dwarf problem, as it is likely that the disk of the Milky Way has been formed by continuous accretion of gas from reservoirs, such as Galactic halo gas and the IGM. However, our simulation already takes into account cosmological gas infall. Hence, the infall model likely does not work for interpretation of the MDF of the dSph. However, we also note that our simulation does not take into account the effect of ionizing radiation fields. If there is a background field, regardless of its specific origin, some fraction of the molecular hydrogen will be photodissociated (Omukai & Nishi 1999; Machacek et al. 2001; Ricotti et al. 2001; Yoshida et al. 2003). As such, our simulation likely overestimates H_2 cooling and, thus, the gas accretion rate.

The MESF model is also unlikely, as it is also fully taken into account in our simulations by introducing the radiative cooling rate depending on the metallicity of the gas particles. This leaves the PIE scenario as the most attractive possibility for solving the G dwarf problem of dSph galaxies. The possible mechanism would be that at high redshift ($z \sim 20$), Population III stars formed at the center of the building blocks and supernova explosions blew up the gas in the building blocks, which helped to enrich the IGM. Then the enriched gas fell back into the system, which became larger after multiple mergers of building blocks, and Population II stars were produced from the enriched gas. If the lifetime of the lowest mass Population III stars is shorter than a Hubble time, Population III stars do not exist in the current dSph. Although the first building blocks have to be large enough ($\sim 10^5$-10^6 $M_\odot$) to make stars (e.g., Tegmark et al. 1997; Abel et al. 1998; Fuller & Couchman 2000; Yoshida et al. 2003), one massive Population III star is enough to blow out the gas (e.g., Bromm et al. 2003). Also, note that the explosion does not have to enrich the IGM of the entire universe; it only needs to enrich the nearby IGM, which falls back into the system. If this is the case, the oldest stars in the dSph have the signature, i.e. abundance pattern, of the first supernova explosion (e.g., Beasley et al. 2003). Hence, low-metallicity stars in dSphs may be the best target for looking for the signature of the first stars (e.g., Sadakane et al. 2004).

Another problem in our simulated galaxy is that its luminosity and velocity dispersion are too low. We have tried different parameter sets of models of star forma-
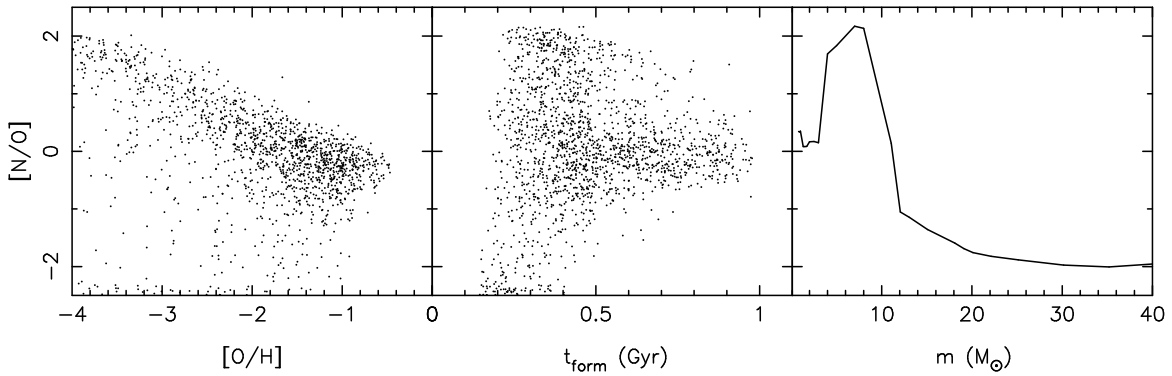
FIG. 10.— *Left*: [N/O] as a function of [O/H] for star particles within $R = 2.5$ kpc. *Middle*: [N/O] as a function of their formation epoch. *Right*: [N/O] yields as a function of the mass of the progenitor stars with metallicity of $Z/Z_\odot = 0.01$ (Woosley & Weaver 1995; van den Hoek & Groenewegen 1997).

tion and SNe feedback. However, we found that to keep metallicity as low as what is observed, strong SNe feedback that leads to a low efficiency of star formation is required, which makes it difficult to produce enough stars at high redshift. The simplest solution is that tens of such small systems merge without any additional star formation. However, this is unlikely, and such mergers make the metallicity gradient shallower (White 1980). Another solution would be to make the galaxy more massive. The virial mass of our galaxy is 5×10^7 M$_\odot$ at $z \sim 6$. Dynamical analysis of dSphs suggests that their mass-to-light ratio is more than 100 (e.g., Kleyna et al. 2001; Hayashi et al. 2003), which suggests that the total mass of the Scl dSph is more than 10^8 M$_\odot$. If the system were big enough, it might be able to continue a low level of star formation even after the re-ionization in the inner region, along scenario 3 described above. If this were the case, it would help to solve "the missing satellite problem" (Klypin et al. 1999; Moore et al. 1999) as discussed in Hayashi et al. (2003); Mashchenko et al. (2005). Admittedly, we have been restricted to the analysis of a single simulation, derived from one initial condition. While this simulation does demonstrate one possible mechanism for explaining the origin of the two distinct populations in the Sculptor dwarf spheroidal, it is critical that the next step in this work entail a suite of simulations at comparable resolution, each with different initial conditions and different patterns of small-scale perturbations. This will allow the analysis of a suite of simulated dwarfs of differing masses and differing assembly histories. Such a suite will allow our preliminary conclusions to be placed on firmer statistical ground, and will allow us to provide further insights into the link between mass, assembly history, and present-day observable characteristics.

Our simulation demonstrates that the recently available detailed properties of the observed dSphs provide invaluable information about their formation history. Our current cosmological simulations obviously miss, or over-simplify, some important physics. For example, our SNe feedback model is too simple, and/or the resolution of our simulation is not good enough to describe SNe feedback, although the present study shows that the effect of SNe would be crucial to explain the observed properties of dSphs. Also, the IMF might depend on the physical condition of the progenitor gas, such as metallicity. In addition, our simulation ignores radiative transfer effects, such as radiative heating and pressure. Strong light from new born stars would suppress cooling of the surrounding gas, which would be important in a small system (Ricotti et al. 2002a,b; Kitayama & Yoshida 2005). Nevertheless, dSphs are good laboratory for studying the physical process of the galaxy formation. We hope that the present study will be a good starting point for testing formation scenarios for dSphs by comparing detailed observations with chemo-dynamical galaxy formation models.

APPENDIX

A. UPDATED VERSION OF GCD+

This study focuses on a small system forming at high redshift, using a high-resolution cosmological simulation. To follow the physics on such small scale, we have updated our original galactic chemodynamical evolution code, `GCD+`. In addition, we have changed some parameter values in the code from our previous studies (e.g., Kawata & Gibson 2003a,b). Below we explain what has been updated.

A.1. *Radiative cooling with non-equilibrium chemical reaction of hydrogen and helium species*

In the updated version, the code follows non-equilibrium chemical reactions of hydrogen and helium species (H, H^+, He, He^+, He^{++}, H_2, H_2^+, H^-) and their cooling processes. We assume ionization equilibrium cooling for radiative cooling of heavy elements, because it is too expensive to follow non-equilibrium chemical reactions of all the ionization states of elements heavier than helium (Omukai 2000). Thus, the total cooling rate is the summation of the equilibrium cooling of heavy elements and non-equilibrium cooling of hydrogen and helium. The equilibrium cooling of heavy elements is calculated using a code based on the Raymond-Smith code (Raymond & Smith 1977), which is used in Cen et al. (1995).

We follow the non-equilibrium chemical reactions of species related to hydrogen and helium, i.e. H, H^+, He, He^+, He^{++}, H_2, H_2^+, H^-, and e^-, and calculate their radiative cooling rate, based on the method of Abel et al. (1997); Anninos et al. (1997). Although Abel et al. (1997) used the molecular hydrogen cooling rate of Lepp & Shull (1983), we adopt an updated one suggested by Galli & Palla (1998). The time-scales of radiative cooling and chemical reaction of these species are much smaller than the dynamical time-scale (Anninos et al. 1997; Yoshida et al. 2003). Therefore, we use sub-time steps to calculate the chemical reaction and integrate the thermal equation. The code considers the time-scale of the chemical reaction to be represented by the time-scale of the change in number of free electrons, $\tau_{\rm sp} = n_{\rm e}/\dot{n}_{\rm e}$. The time-scale for radiative cooling is calculated by $\tau_{\rm rad} = e/|\Lambda - \Gamma|$, where e is thermal energy, and Λ and Γ are the cooling and heating[8] rate, respectively. For each gas particle i, we set the sub-time step to be $\Delta t_{{\rm sub},i} = \tau_{\rm dyn}/2^n \leq \min(\epsilon\tau_{\rm sp}, \epsilon\tau_{\rm rad})$ with $\epsilon = 0.1$, for efficient integration. Here $\tau_{\rm dyn}$ is the minimum time step required from dynamical evolution, $\Delta t_{\rm dyn}$ (Kawata 1999). Following Anninos et al. (1997), we update the number $n_{k,i}$ of the k-th species in a gas particle i by a backward differentiation method, $n_{k,i}^{t+\Delta t_{{\rm sub},i}} = (C_{k,i}^{t+\Delta t_{{\rm sub},i}}\Delta t_{{\rm sub},i}+n_{k,i}^t)/(1+D_{k,i}^{t+\Delta t_{{\rm sub},i}}\Delta t_{{\rm sub},i})$. Here, $C_{k,i}$ and $D_{k,i}$ are the creation and destruction rates, respectively. The thermal energy is updated by a semi-implicit method in our code. Note that Anninos et al. (1997) use the explicit method. However, we find that the semi-implicit method is more robust (K. Yoshikawa 2003, private communication). We solve the following equation with iteration:

$$u_i^{t+\Delta t_{{\rm sub},i}} = u_i^t + \Delta t_{{\rm sub},i}\frac{\Delta E_{{\rm SN},i}(t_n,\Delta t_{\rm dyn})}{\Delta t_{\rm dyn}} + 0.5\Delta t_{{\rm sub},i}\left[\left(\frac{du}{dt}\right)_{{\rm ad},i}^{t_n} + \left(\frac{du}{dt}\right)_{{\rm ad},i}^{t_n+\Delta t_{\rm dyn}} + \frac{\Gamma_i^t - \Lambda_i^t}{\rho_{{\rm g},i}} + \frac{\Gamma_i^{t+\Delta t_{{\rm sub},i}} - \Lambda_i^{t+\Delta t_{{\rm sub},i}}}{\rho_{{\rm g},i}}\right].$$
(A1)

Here, $\Delta E_{{\rm SN},i}(t_n,\Delta t_{\rm dyn})$ is the heating energy from SNe within the dynamical time step from t_n which indicates the time at the beginning of this sub-time step integration. Also, $(du/dt)_{{\rm ad},i}$ is the adiabatic term (Kawata 1999) for the thermal equation. Since $(du/dt)_{{\rm ad},i}$ requires a neighbor particle search, which is computationally expensive, we use a mean value of $(du/dt)_{{\rm ad},i}$ at $t = t_n$ and $t = t_n + \Delta t_{\rm dyn}$. Thus, the code re-calculates only the radiative cooling and heating terms at the sub-time step, $t + \Delta t_{{\rm sub},i}$, i.e. $\Gamma_i^{t+\Delta t_{{\rm sub},i}}$ and $\Lambda_i^{t+\Delta t_{{\rm sub},i}}$, and the other terms are fixed. In addition, for simplicity we assume that the gas density does not change dramatically within $\Delta t_{\rm dyn}$; i.e., the gas density is assumed to be constant with $\rho_{{\rm g},i}^{t_n+\Delta t_{\rm dyn}}$ during these sub-time steps.

A.2. *Yields*

It is well known that the iron yield suggested in Woosley & Weaver (1995) seems to be overestimated and leads to much lower $[\alpha/{\rm Fe}]$ values, compared to those observed in low-metallicity stars in the solar neighborhood. Since the iron yield is the most ambiguous yield for the SNe II nucleosynthesis model, it has been discussed that the half of Woosley & Weaver's suggested yield is more appropriate (e.g., Timmes et al. 1995). Therefore, the updated code adopts half of the yield of iron in Woosley & Weaver (1995).

A.3. *Star formation criteria*

The criteria of star formation are also changed from what were adopted in Kawata & Gibson (2003a). In the updated code, the Jeans unstable condition and density threshold are excluded from the criteria. Instead, we introduced a new criterion that the cooling time has to be smaller than the dynamical time, i.e. $t_{\rm cool} = e/|\Lambda - \Gamma| < t_{\rm dyn} = \sqrt{3\pi/16G\rho}$ and $\Lambda > \Gamma$. Finally, this cooling time criterion and the convergence of the gas velocity field, $\nabla \cdot \boldsymbol{v}_i < 0$, are the criteria for star formation in the updated code. The Jeans unstable condition is discarded, because it is sensitive to the numerical resolution (Okamoto et al. 2003). The density threshold is ignored, because it is not well understood whether or not there is such threshold, except for disk galaxies. In addition, for disk galaxies the density threshold explained by the dynamical instability condition of the rotating gas disk (Kennicutt 1989), which should be able to be naturally taken into account in dynamical simulations.

REFERENCES

Abel, T., Anninos, P., Norman, M. L., & Zhang, Y. 1998, ApJ, 508, 518

Abel, T., Anninos, P., Zhang, Y., & Norman, M. L. 1997, New Astronomy, 2, 181

Anninos, P., Zhang, Y., Abel, T., & Norman, M. L. 1997, New Astronomy, 2, 209

Arimoto, N., & Yoshii, Y. 1987, A&A, 173, 23

Arnone, E., Ryan, S. G., Argast, D., Norris, J. E., & Beers, T. C. 2005, A&A, 430, 507

Baade, W. 1944, ApJ, 100, 137

Beasley, M. A., Kawata, D., Pearce, F. R., Forbes, D. A., & Gibson, B. K. 2003, ApJ, 596, L187

Benson, A. J., Frenk, C. S., Lacey, C. G., Baugh, C. M., & Cole, S. 2002, MNRAS, 333, 177

[8] In this paper, we do not take into account any background radiation. Thus, there is no photo-ionization heating.

Bertschinger, E. 2001, ApJS, 137, 1

Bressan, A., Chiosi, C., & Fagotto, F. 1994, ApJS, 94, 63

Bromm, V., Yoshida, N., & Hernquist, L. 2003, ApJ, 596, L135

Bullock, J. S., Kravtsov, A. V., & Weinberg, D. H. 2000, ApJ, 539, 517

Carlberg, R. G. 1984, ApJ, 286, 403

Carraro, G., Chiosi, C., Girardi, L., & Lia, C. 2001, MNRAS, 327, 69

Cen, R., Kang, H., Ostriker, J. P., & Ryu, D. 1995, ApJ, 451, 436

Chiba, M., & Nath, B. B. 1994, ApJ, 436, 618

Dekel, A., & Silk, J. 1986, ApJ, 303, 39

Efstathiou, G. 1992, MNRAS, 256, 43P

Fuller, T. M., & Couchman, H. M. P. 2000, ApJ, 544, 6

Gallagher, J. S., & Wyse, R. F. G. 1994, PASP, 106, 1225

Galli, D., & Palla, F. 1998, A&A, 335, 403

Geisler, D., Smith, V. V., Wallerstein, G., Gonzalez, G., & Charbonnel, C. 2005, AJ, 129, 1428

Gibson, B. K. 1997, MNRAS, 290, 471

Grebel, E. K. 1997, Reviews of Modern Astronomy, 10, 29

Greggio, L. 1997, MNRAS, 285, 151

Greggio, L., & Renzini, A. 1983, A&A, 118, 217

Hayashi, E., Navarro, J. F., Taylor, J. E., Stadel, J., & Quinn, T. 2003, ApJ, 584, 541

Ikuta, C., & Arimoto, N. 2002, A&A, 391, 55

Kawata, D. 1999, PASJ, 51, 931

Kawata, D., & Gibson, B. K. 2003a, MNRAS, 340, 908

—. 2003b, MNRAS, 346, 135

Kennicutt, R. C. 1989, ApJ, 344, 685

Kitayama, T., & Suto, Y. 1996, ApJ, 469, 480

Kitayama, T., & Yoshida, N. 2005, ApJ, 630, 675

Kleyna, J. T., Wilkinson, M. I., Evans, N. W., & Gilmore, G. 2001, ApJ, 563, L115

Klypin, A., Kravtsov, A. V., Valenzuela, O., & Prada, F. 1999, ApJ, 522, 82

Kobayashi, C. 2004, MNRAS, 347, 740

Kobayashi, C., & Arimoto, N. 1999, ApJ, 527, 573

Kobayashi, C., Tsujimoto, T., & Nomoto, K. 2000, ApJ, 539, 26

Kodama, T., & Arimoto, N. 1997, A&A, 320, 41

Kunkel, W. E., & Demers, S. 1977, ApJ, 214, 21

Lanfranchi, G. A., & Matteucci, F. 2003, MNRAS, 345, 71

—. 2004, MNRAS, 351, 1338

Lanfranchi, G. A., Matteucci, F., & Cescutti, G. 2005, ArXiv Astrophysics e-prints

Larson, R. B. 1974, MNRAS, 166, 585

Lepp, S., & Shull, J. M. 1983, ApJ, 270, 578

Machacek, M. E., Bryan, G. L., & Abel, T. 2001, ApJ, 548, 509

Mashchenko, S., Couchman, H. M. P., & Sills, A. 2005, ApJ, 624, 726

Mateo, M. L. 1998, ARA&A, 36, 435

McWilliam, A., & Smecker-Hane, T. A. 2005a, in ASP Conf. Ser. 336: Cosmic Abundances as Records of Stellar Evolution and Nucleosynthesis, 221–+

McWilliam, A., & Smecker-Hane, T. A. 2005b, ApJ, 622, L29

Mo, H. J., & White, S. D. M. 1996, MNRAS, 282, 347

Moore, B., Ghigna, S., Governato, F., Lake, G., Quinn, T., Stadel, J., & Tozzi, P. 1999, ApJ, 524, L19

Mori, M., Ferrara, A., & Madau, P. 2002, ApJ, 571, 40

Ogorodnikov, K. F. 1965, Dynamics of stellar systems (Oxford: Pergamon, 1965, edited by Beer, Arthur)

Okamoto, T., Jenkins, A., Eke, V. R., Quilis, V., & Frenk, C. S. 2003, MNRAS, 345, 429

Omukai, K. 2000, ApJ, 534, 809

Omukai, K., & Nishi, R. 1999, ApJ, 518, 64

Raiteri, C. M., Villata, M., & Navarro, J. F. 1996, A&A, 315, 105

Raymond, J. C., & Smith, B. W. 1977, ApJS, 35, 419

Ricotti, M., & Gnedin, N. Y. 2005, ApJ, 629, 259

Ricotti, M., Gnedin, N. Y., & Shull, J. M. 2001, ApJ, 560, 580

—. 2002a, ApJ, 575, 33

—. 2002b, ApJ, 575, 49

Sadakane, K., Arimoto, N., Ikuta, C., Aoki, W., Jablonka, P., & Tajitsu, A. 2004, PASJ, 56, 1041

Shetrone, M., Venn, K. A., Tolstoy, E., Primas, F., Hill, V., & Kaufer, A. 2003, AJ, 125, 684

Smecker-Hane, T. A., & McWilliam, A. 2002, astro-ph, 0205411

Spergel, D. N., Verde, L., Peiris, H. V., Komatsu, E., Nolta, M. R., Bennett, C. L., Halpern, M., Hinshaw, G., Jarosik, N., Kogut, A., Limon, M., Meyer, S. S., Page, L., Tucker, G. S., Weiland, J. L., Wollack, E., & Wright, E. L. 2003, ApJS, 148, 175

Susa, H., & Umemura, M. 2004a, ApJ, 600, 1

—. 2004b, ApJ, 610, L5

Tegmark, M., Silk, J., Rees, M. J., Blanchard, A., Abel, T., & Palla, F. 1997, ApJ, 474, 1

Thoul, A. A., & Weinberg, D. H. 1996, ApJ, 465, 608

Timmes, F. X., Woosley, S. E., & Weaver, T. A. 1995, ApJS, 98, 617

Tinsley, B. M. 1975, ApJ, 197, 159

Tolstoy, E. 2005, astro-ph, 0506481

Tolstoy, E., Irwin, M. J., Helmi, A., Battaglia, G., Jablonka, P., Hill, V., Venn, K. A., Shetrone, M. D., Letarte, B., Cole, A. A., Primas, F., Francois, P., Arimoto, N., Sadakane, K., Kaufer, A., Szeifert, T., & Abel, T. 2004, ApJ, 617, L119

Tolstoy, E., Venn, K. A., Shetrone, M., Primas, F., Hill, V., Kaufer, A., & Szeifert, T. 2003, AJ, 125, 707

van den Bergh, S. 1962, AJ, 67, 486

van den Hoek, L. B., & Groenewegen, M. A. T. 1997, A&AS, 123, 305

White, S. D. M. 1980, MNRAS, 191, 1P

White, S. D. M., & Rees, M. J. 1978, MNRAS, 183, 341

Woosley, S. E., & Weaver, T. A. 1995, ApJS, 101, 181

Yoshida, N., Abel, T., Hernquist, L., & Sugiyama, N. 2003, ApJ, 592, 645